Stabilization of the tetragonal distortion of Fe_xCo_{1-x} alloys by C impurities: A potential new permanent magnet

E. K. Delczeg-Czirjak,[1] A. Edström,[1] M. Werwiński,[1] J. Rusz,[1,*] N. V. Skorodumova,[1,2] L. Vitos,[1,3,4] and O. Eriksson[1]

[1]*Division of Materials Theory, Department of Physics and Astronomy, Uppsala University, Box 516, SE-751 20, Uppsala, Sweden*

[2]*Multiscale Materials Modelling, Department of Materials Science and Engineering, Royal Institute of Technology (KTH), SE-100 44 Stockholm, Sweden*

[3]*Applied Materials Physics, Department of Materials Science and Engineering, Royal Institute of Technology (KTH), SE-100 44 Stockholm, Sweden*

[4]*Research Institute for Solid State Physics and Optics, Wigner Research Center for Physics, P.O. Box 49, HU 1525 Budapest, Hungary*

(Received 31 August 2013; revised manuscript received 10 March 2014; published 2 April 2014)

We have analyzed by density functional theory calculations the structural and magnetic properties of Fe-Co alloys doped by carbon. In analogy with the formation of martensite in steels we predict that such a structure also forms for Fe-Co alloys in a wide range of concentrations. These alloys are predicted to have a stable tetragonal distortion, which in turn leads to an enhanced magnetocrystalline anisotropy energy of up to 0.75 MJ/m^3 and a saturated magnetization field of 1.9 T.

DOI: 10.1103/PhysRevB.89.144403 PACS number(s): 75.50.Ww, 75.30.Gw, 75.50.Bb, 71.15.Nc

I. INTRODUCTION

Devices utilizing permanent magnet materials for their functionality are ubiquitous. Typical applications include utilization of the tractive or repelling mechanical forces between magnetic materials or conversion of mechanical energy to electrical energy and vice versa. In information technologies permanent magnets are used, for example, in data storage. Quality and performance of permanent magnet materials are characterized by several quantities, energy product being among the most important ones. The energy product, in turn, is influenced by the magnetocrystalline anisotropy energy (MAE) and saturation magnetization M_s, which are both accessible from first-principles calculations. The highest-energy product is typically achieved in magnets based on rare-earth elements, in particular the neodymium ($Nd_2Fe_{14}B$) and samarium ($SmCo_5$) magnets. However, a steep rise in and volatility of the prices of the rare-earth elements in the last decade have initiated intensive research efforts worldwide to develop alternative materials for permanent magnet applications, especially those that contain very little or no rare-earth elements. Hence, attention has been given to the magnetic anisotropy of, e.g., Fe_2P [1,2], Fe/W-Re multilayers [3], FeNi [4], or Fe-Co-B alloys [5].

Burkert *et al*. [6] predicted a huge MAE in tetragonally distorted iron-cobalt alloys. A MAE reaching 0.7–0.8 meV/atom was predicted in materials composed of approximately 60% cobalt and 40% iron with a tetragonal distortion of $c/a \approx 1.2$. Experimentally, it is not easy to grow Fe-Co alloys with such high tetragonal distortion because their natural structure is bcc. Nevertheless, the system was experimentally realized by an epitaxial growth on various substrates [7–9], and an enhanced value of MAE was confirmed, although in experiments it did not reach the theoretically predicted peak value. Later theoretical studies, which included more realistic treatments of the chemical disorder [10,11] present in Fe-Co alloys, have corrected the theoretical MAE to values that are very close to the experimental ones.

In this work we explored an alternative way of stabilizing the tetragonal distortion in Fe-Co alloys, namely, by alloying it with carbon.

A metastable martensite phase of the $Fe_{1-x}C_x$ system is widely known [12–14]: by a rapid quenching of austenite, which crystallizes in a fcc structure, a martensite forms in a body-centered tetragonal (bct) structure. In the martensite one can dissolve up to about 0.8 wt %, that is, 3.5 at. %, of carbon. Due to the long-range interaction between the strain field around the carbon atoms in the Fe matrix, C preferentially occupies a specific octahedral interstitial position of a bcc lattice (see Fig. 1). The level of tetragonal distortion of the martensite, expressed via the c/a ratio, is experimentally found to be proportional to the amount of carbon in the alloy [15–17], following the relations

$$\begin{aligned} c/a &= 1 + \gamma x, \\ c &= a_0 + \alpha x, \\ a &= a_0 - \beta x, \end{aligned} \tag{1}$$

where γ is 0.046 ± 0.001 and x is the wt % of C, $a_0 = 2.87$ Å is the lattice parameter of bcc Fe, $\alpha = (0.116 \pm 0.002)$ Å, and $\beta = (0.013 \pm 0.002)$ Å.

The Fe-C and Fe-Co-C phase diagrams display several similarities. In particular, the stable phase of Fe-Co-C is again fcc, and it can dissolve up to about 2 wt % of C [18–21]. Although martensite formation in a quenched Fe-Co-C system has not yet been reported experimentally, in analogy with Fe-C alloys, we expect the appearance of a metastable bct phase in rapidly cooled Fe-Co-C alloys for a wide range of Fe-Co concentrations.

Here we utilize first-principles electronic structure calculations to identify the stationary bct structures of Fe-Co-C alloys and evaluate the corresponding MAE energies. Several different *ab initio* codes were used at particular phases of this work based on their performance, accuracy, and set of features.

*Corresponding author: jan.rusz@physics.uu.se

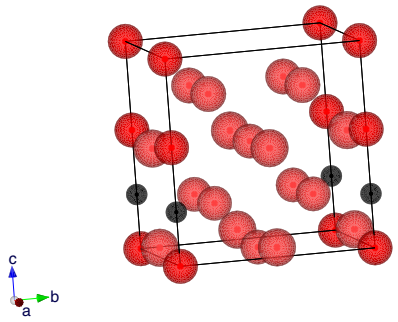

FIG. 1. (Color online) Interstitial C atom (small dark spheres) in relaxed $Fe_{16}C$. Note the local distortion of the positions of Fe atoms (larger red spheres) near the position of the C atom.

II. METHODS

In the first step, three Fe_yC supercells were prepared to model three different C concentrations. In particular, we have generated $1 \times 2 \times 2, 2 \times 2 \times 2$, and $2 \times 2 \times 3$ supercells representing Fe_8C, $Fe_{16}C$, and $Fe_{24}C$, respectively. The Fe atoms occupied the ideal bcc positions in all supercells, and one C atom was placed in the $(00\frac{1}{2})$ position of a regular bcc lattice. These structures were fully relaxed using the conjugate-gradient algorithm as implemented in the VIENNA AB INITIO SIMULATION PACKAGE (VASP) [22–25]. We have used the generalized gradient approximation (GGA) [26] for the exchange-correlation potential. The Monkhorst-Pack **k**-point mesh [27] was set to $16 \times 16 \times 8, 8 \times 8 \times 8$, and $8 \times 8 \times 6$ for Fe_8C, $Fe_{16}C$, and $Fe_{24}C$, respectively. The plane-wave cutoff and the energy convergence criterion were set to 500 eV and 10^{-7} eV, respectively. The spin-orbit coupling was neglected.

In the next step, these relaxed structures were used as an input for the exact muffin-tin orbitals–full charge density (EMTO-FCD) method [28–34]. The chemical disorder was treated via the coherent potential approximation (CPA) [35,36]. The one-electron equations were solved within the scalar-relativistic and soft-core approximations. The Green's functions were calculated for 18 complex energy points distributed exponentially on a semicircular contour with a radius of 0.6 Ry. The $3d$ and $4s$ states of Fe, Co, and Ni, the $3s$ and $3p$ states of Al, and the $2s$ and $2p$ states of C were treated as valence electrons. The s, p, d, and f orbitals ($l_{\max} = 3$) were included in the muffin-tin basis set. The one center expansion of the full-charge density was truncated at $l^h_{\max} = 8$. In the irreducible wedge of the Brillouin zones 40–200 uniformly distributed **k** points were used. We described the electrostatic correction to the single-site CPA, for the case of solid solutions, using the screened impurity model [37] with a screening parameter of 0.6.

As a final step in our investigation, we used the stable structure models identified by EMTO-FCD calculations as an input for the evaluation of the MAE. For that purpose we have used two different approaches to the treatment of substitutional disorder: a virtual crystal approximation (VCA) and a relativistic CPA. VCA has been reported to give a qualitatively correct behavior for the MAE of Fe-Co alloys [10,11], although it was also observed that the MAE was significantly overestimated by a factor of 3 to 4. In the calculations of Fe-Co alloys reported so far, the relaxation of the internal coordinates has not been considered. Therefore we decided to apply both approaches, VCA and CPA, to evaluate the MAE of the structure models distorted by the presence of C atom.

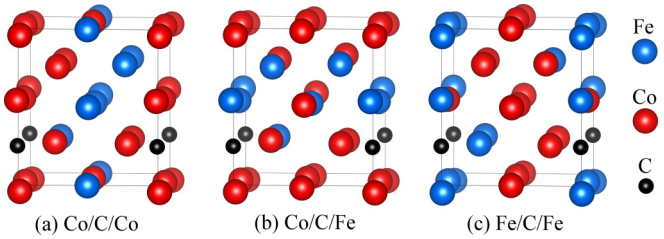

FIG. 2. (Color online) Optimized SQS models of $Fe_6Co_{10}C$ with three different placements of C atoms.

For VCA calculations we chose a full-potential all-electron code that includes spin-orbital coupling, namely, WIEN2K [38]. WIEN2K uses a full-potential linearized augmented plane-wave basis set. As in the calculations discussed above, we used GGA [26] for the exchange-correlation potential. Spin-orbit coupling was included via a second-variational approach. The MAE values were obtained by the magnetic force theorem [39], where the sums of Kohn-Sham eigenvalues for occupied states are compared for different magnetization directions. We have used 2600, 1200, and 1000 **k** points for the $y = 8$, $y = 16$, and $y = 24$ Fe_yC systems, respectively, and the Brillouin-zone integration was performed using the modified tetrahedron method [22]. The smallest muffin-tin radius times maximum **k** vector was set to $RK_{\max} = 8$ in all cases.

For relativistic CPA calculations we have employed the spin polarized relativistic Korringa-Kohn Rostoker (SPR-KKR) code [40]. The electronic structure for the optimized structures was evaluated using the GGA. MAE was calculated as a difference of total energies for the two magnetization directions, without considering full-potential effects. The basis set consisted of s, p, d, and f orbitals, and the number of **k** points was 10 000.

In addition to the workflow described above, we have also performed a limited set of supercell calculations using the WIEN2K code. A Fe_6Co_{10} special quasirandom structure (SQS) [41] was generated using stochastic Monte Carlo methods with the code ATAT [42]. Then a single C atom was introduced at different positions of the supercell along Fe-Fe, Fe-Co, or Co-Co bonds. All these structures were independently relaxed in terms of both lattice parameters and internal atomic positions. The optimized SQS models are shown in Fig. 2. Finally, MAE was evaluated as a total-energy difference for two magnetization directions with a **k** mesh of $13 \times 13 \times 11$ and $RK_{\max} = 7.0$, which were tested to provide well-converged values.

III. RESULTS AND DISCUSSION

A. Stabilization of the tetragonal structure

As the first step, we have evaluated the total energies of pure Fe_yC systems for the structures relaxed by VASP. In Table I we summarize the c/a ratio and equilibrium volume V_{eq} obtained by VASP and EMTO calculations and the estimated values, assuming that relations presented in Eq. (1) hold for higher carbon content too. The equilibrium c/a ratio $(c/a)_{\text{eq}}$ obtained

TABLE I. Equilibrium c/a ratios and volumes V of Fe_yC systems extrapolated from the experimentally observed relation, Eq. (1), compared to the present theoretical results.

		$(c/a)_{eq}$			V_{eq} (Å^3)		
Alloy	wt % C	Expt.	VASP	EMTO	Expt.	VASP	EMTO
Fe_8C	2.6	1.12	1.11	1.13	102	100	102
$Fe_{16}C$	1.3	1.06	1.08	1.07	196	196	195
$Fe_{24}C$	0.8	1.04	1.04	1.04	291	286	287

by EMTO agreed well with the VASP calculations and with the estimated values, giving us confidence to proceed with the evaluation of total energies for Fe-Co-C alloys.

It should be noted that in the case of a disordered alloy, the structural model might depend on the local surrounding of the C atom. To get an upper estimate of the importance of these effects, we have considered a small $1 \times 1 \times 2$ supercell using VASP. The theoretical $(c/a)_{eq}$ for Fe_4C is equal to 1.16. Substitutional addition of 50 at. % Co on the Fe sites leads to the following two extreme configurations: in the first one there is an Fe-C-Fe chain along the c axes and in the second one a Co-C-Co chain. The c/a-ratio shift in the first case is 0.06, i.e., $(c/a)_{Fe-C-Fe} = 1.23$. When C atoms are accommodated in between the two Co atoms along c axes, the increase in the c/a ratio compared to Fe_4C is reduced, i.e., $(c/a)_{Co-C-Co} = 1.18$. The latter configuration is more stable, having a total energy lower by 0.2 eV (15 mRy) per cell compared to the first one. This result indicates that the preferred position of C atoms in the lattice is nearby Co atoms. The preferentiality of the C atom being near Co atoms will be revisited later in the context of the SQS supercells. It will be shown that the total-energy differences are reduced at lower C concentrations.

The effect of Co doping on the phase stability of Fe_yC has been investigated using the EMTO method and is summarized in Table II. At the highest concentration of carbon (for $y = 8$, i.e., 11.11 at. % of C), the desired c/a ratio [6] of $\sim$1.2 is obtained by the addition of about 30 at. % of Co. Increasing further the Co content to 50 at. % destabilizes the local energy minimum and moves it towards large values ($c/a > 1.3$) in proximity to the fcc structure. This can be explained by a softening of the lattice by the addition of Co. The elastic constant associated with the distortion of the bcc lattice via bct towards fcc suddenly decreases as the Co content is increased over 30 at. % [43]. This suggests that lower C content in $Fe_{1-x}Co_x$($0.54 \leqslant x \leqslant 0.65$ at. %) could still be sufficient to stabilize a c/a ratio favorable for a large value of MAE. This is important because $(Fe_{1-x}Co_x)_8C$ contains $\sim$2.5 wt % of C, which is most likely too high for a martensite phase, at least for iron-rich alloys.

TABLE II. Calculated equilibrium structure parameters of Fe-Co-C alloys for selected concentrations of Co and C atoms.

Composition	$(c/a)_{eq}$	a (Å)
$(Fe_{0.7}Co_{0.3})_8C$	1.174	2.777
$(Fe_{0.5}Co_{0.5})_8C$	>1.3	
$(Fe_{0.4}Co_{0.6})_{16}C$	1.124	2.766
$(Fe_{0.39}Co_{0.61})_{16}C$	1.129	2.762
$(Fe_{0.35}Co_{0.65})_{16}C$	1.165	2.729
$(Fe_{0.4}Co_{0.6})_{24}C$	1.033	2.834
$(Fe_{0.35}Co_{0.65})_{24}C$	1.036	2.829
$(Fe_{0.35}Co_{0.6}Al_{0.05})_{16}C$	1.152	2.747
$(Fe_{0.39}Co_{0.6}Ni_{0.01})_{16}C$	1.132	2.759
$(Fe_{0.35}Co_{0.6}Ni_{0.05})_{16}C$	>1.3	

Reducing the amount of carbon to 5.88 at. %, we reach more realistic concentrations, from an experimental viewpoint. Moreover, as anticipated above, it appears to be possible to stabilize higher concentrations of Co, close to the desired 60 at. %. Total-energy surfaces of $(Fe_{1-x}Co_x)_{16}C$ for $x = 0$, 0.6, 0.61, and 0.65 are shown in Fig. 3. For the pure iron martensite the c/a ratio is 1.07 (see also Table I), but for Co concentrations $x = 0.60$ and 0.61 the local energy minima move to higher c/a ratios of 1.124 and 1.129. By adding more Co this local minimum gradually destabilizes and moves towards the fcc structure.

By reducing the carbon concentration further, the effect of Co doping in $Fe_{24}C$ becomes less significant than in systems with higher C content: the stationary c/a ratio stays between 1.03 and 1.04 up to over 60 at. % of Co (see Table II).

First-principles calculations have shown that Ni and Al impurities in $Fe_{16}C$ have a strong bct stabilizing effect [44]. Therefore, we tested their influence on the structure of Fe-Co-C alloys. Substitution of Fe with a small amount of Ni or Al into $(Fe_{0.4}Co_{0.6})_{16}C$ indeed appears to further increase the c/a ratio (see Table II). However, the calculated total energy versus c/a ratio has only a shallow minimum, suggesting that it may be difficult to stabilize this minimum configuration experimentally. In the further considerations we will therefore limit ourselves to the C-doped Fe-Co alloys without other elements.

B. Saturation magnetization and magnetocrystalline anisotropy energy

In this section we describe our VCA, CPA, and supercell results of the saturation magnetization and MAE calculations. Table III summarizes the MAE calculated with VCA for $(Fe_{1-x}Co_x)_yC$ with various values of x and y identified by the EMTO method. We find that most of the studied systems result in MAE values corresponding to that of hcp Co (0.95 MJ/m^3), but a value approximately twice as large is found for $(Fe_{0.35}Co_{0.65})_{16}C$. The saturation magnetization of these alloys is higher than that of hcp Co ($\mu_0 M_s = 1.63$ T).

Values of the MAE around 800 μeV/atom [6] were not obtained by addition of interstitial carbon for several reasons. First of all, the optimal ratio of $c/a \approx 1.2$ was not reached for Co concentration of $x \approx 0.6$. Second, the interstitial carbon causes some local structural disorder, and its presence also influences the electronic structure via hybridization effects. We illustrate this for the $(Fe_{0.4}Co_{0.6})_{16}C$ system in Fig. 4. In Fig. 4 we compare spin-up bands of $(Fe_{0.4}Co_{0.6})_{16}C$ with bands of $Fe_{0.4}Co_{0.6}$. Note that the presence of carbon causes a splitting of the bands, notably around the Γ point, where a band degeneracy is lifted. Carbon also introduces new bands, some of which hybridize with nearby Fe and Co states. To evaluate the influence of carbon atom on MAE, we have calculated the MAE of Fe-Co alloys with the same structural parameters as the Fe-Co-C alloys from Table II, but without carbon and distortion. [Note that in previous studies of Fe-Co-alloys [6,7,10], volume effects were not considered. The unit cells

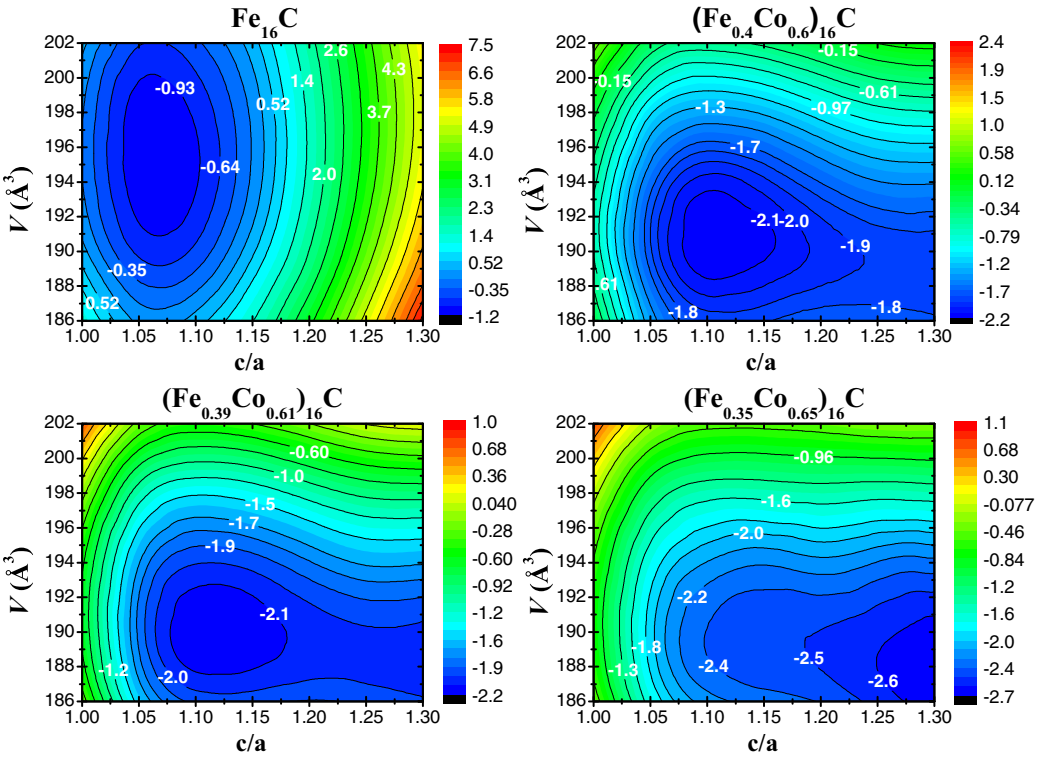

FIG. 3. (Color online) Contour plot of total energy (mRy/atom) as a function of unit-cell volume V and c/a ratio for $(Fe_{1-x}Co_x)_{16}C$.

of all the $(Fe_{1-x}Co_x)_yC$ systems studied here have a volume per Fe-Co atom a few percent larger than the equilibrium volume in pure Fe-Co systems without carbon; therefore direct comparison of previously published results with the data presented here is not possible.] We observe a tendency of the MAE to be lower in $(Fe_{1-x}Co_x)_yC$ than predicted from calculations for $Fe_{1-x}Co_x$, although qualitative trends and orders of magnitude are preserved. However, even without reaching the earlier predicted maxima, these values represent a significant increase of MAE relative to values expected for pure Fe-Co systems with cubic symmetry. Assuming that one could synthesize these materials in bulk quantities, it would make these Fe-Co-C alloys potentially interesting candidates for replacement materials for permanent magnet applications.

As for the magnetic moment, it is, on average, lower in the $(Fe_{1-x}Co_x)_yC$ systems than in alloys without carbon. Further analysis of magnetic moments from CPA calculations reveals that the Fe and Co atoms close to the carbon atom have reduced magnetic moment down to values of $1.90\mu_B$ and $1.13\mu_B$, respectively, in agreement with the moment of the corresponding virtual atom from WIEN2K, $1.45\mu_B$. Those farther away reach values of $2.64\mu_B$ and $1.71\mu_B$ for Fe and Co, respectively ($2.2\mu_B$ in VCA).

However, it is likely that MAE values obtained by VCA are overestimated, as was pointed out before [10,11]. Therefore we have recalculated MAE of some of the structures also using the relativistic CPA method implemented in SPR-KKR [40]. Due to substantially increased computational demands of CPA calculations, we have not recalculated all the alloys of Table III; only four were selected.

Comparing the CPA results in Table IV to VCA results from Table III, we observe that the MAE values of $(Fe_{0.7}Co_{0.3})_8C$ are remarkably similar, differing less than 10%. When comparing the MAE values for structures without carbon, the difference is approximately a factor of 2. It is tempting to suggest that the MAE for this system is dictated more by structural distortion in the presence of carbon than by the overall c/a distortion of an otherwise perfect bct structure. This would be supported

TABLE III. Lattice parameters, magnetocrystalline anisotropy energy, and magnetic moments for various $(Fe_{1-x}Co_x)_yC$ systems, as well as for equivalent $Fe_{1-x}Co_x$ systems with the same lattice parameters but no carbon atoms, using WIEN2K VCA.

							No carbon	
Composition	c/a	a (Å)	MAE ($\frac{\mu eV}{atom}$)	MAE ($\frac{MJ}{m^3}$)	m ($\frac{\mu_B}{atom}$)	$\mu_0 M_S$ (T)	MAE ($\frac{\mu eV}{atom}$)	m ($\frac{\mu_B}{atom}$)
$(Fe_{0.7}Co_{0.3})_8C$	1.174	2.777	76.5	1.10	1.88	1.96	54.0	2.42
$(Fe_{0.4}Co_{0.6})_{16}C$	1.124	2.766	90.2	1.29	1.87	1.95	222.0	2.16
$(Fe_{0.39}Co_{0.61})_{16}C$	1.129	2.762	85.3	1.22	1.80	1.87	236.3	2.15
$(Fe_{0.35}Co_{0.65})_{16}C$	1.165	2.729	133.5	1.92	1.82	1.91	353.9	2.10
$(Fe_{0.4}Co_{0.6})_{24}C$	1.033	2.834	42.8	0.61	1.98	2.04	46.7	2.17
$(Fe_{0.35}Co_{0.65})_{24}C$	1.036	2.829	52.0	0.74	1.94	2.00	48.2	2.12

TABLE IV. Magnetocrystalline anisotropy energy and magnetic moments for various $(Fe_{1-x}Co_x)_yC$ systems, as well as for equivalent $Fe_{1-x}Co_x$ systems with the same lattice parameters but no carbon atoms. Calculated with SPR-KKR using CPA.

			No carbon			
Composition	MAE ($\frac{\mu eV}{atom}$)	m ($\frac{\mu_B}{atom}$)	MAE ($\frac{\mu eV}{atom}$)	m_{Fe} ($\frac{\mu_B}{atom}$)	m_{Co} ($\frac{\mu_B}{atom}$)	m_{avg} ($\frac{\mu_B}{atom}$)
$(Fe_{0.7}Co_{0.3})_8C$	80.8	1.85	27.1	2.69	1.83	2.43
$(Fe_{0.4}Co_{0.6})_{16}C$	41.6	1.82	79.7	2.69	1.81	2.16
$(Fe_{0.39}Co_{0.61})_{16}C$		1.81	77.7	2.69	1.80	2.15
$(Fe_{0.35}Co_{0.65})_{16}C$	30.2	1.76	71.0	2.67	1.77	2.09

also by comparing the CPA values of MAE for structures with and without carbon, respectively, the latter being lower.

The picture, however, changes for the reduced concentration of C atoms. The MAE calculated by CPA is reduced by a factor of 2.2 and 4.4, respectively, compared to VCA results. This factor corresponds well to recently published results [10]. The reduction factor is also more or less the same for the structure models without carbon. Thus we conclude that at this concentration level the MAE is actually reduced by structural distortion. The largest MAE is obtained for the structure with 40 at. % of Fe, namely, 0.59 MJ/m^3, about a factor of 3 lower than the highest VCA prediction.

However, both VCA and CPA are missing an additional source of disorder. The initial tests of small supercells discussed above indicated that if a C atom is located between two Co atoms, the structural distortion is smaller compared to a model with a C atom between two Fe atoms. Likewise, in a larger structural model one can expect that a C atom placed between two Co atoms causes the smallest displacements of atoms in the local neighborhood. These effects cannot be captured by VCA or CPA, both of which are single-site models of a disordered structure.

To probe the dependence of the MAE on the chemical neighborhood of the C atom we have constructed a SQS model of $Fe_6Co_{10}C$ ($x = 0.625$), where the C atom was placed between two Co atoms or between Co and Fe atoms or between two Fe atoms. These three structure models were fully relaxed (Fig. 2). The total-energy differences between them were less than 10 ± 2 mRy per supercell, with the case where C is between two Co atoms being the lowest. As anticipated, this energy difference is somewhat reduced compared to our initial checks with $(Fe_{0.5}Co_{0.5})_4C$, suggesting that all environments for the C atom are likely to be realized at room temperature. However, the difference of relaxed c/a ratios for these three models is small, with $c/a = 1.12 \pm 0.01$ in all three cases. Similarly, the total magnetization shows very little variation, $1.80 \pm 0.01 \mu_B$ per atom. For all three structure models we have evaluated the MAE as a total-energy difference for the two magnetization directions, and the results were also rather close to each other, reaching a value of 51 ± 9 μeV/atom $= 0.75 \pm 0.13$ MJ/m^3. These values are larger than the highest MAE predicted by CPA for the same C concentration (41.6 μeV/atom), indicating the importance of the local species-dependent lattice distortion for the precise value of MAE. At the same time, they suggest that the dependence of the overall magnetic characteristics on the specific placement of the impurity atom is not strong.

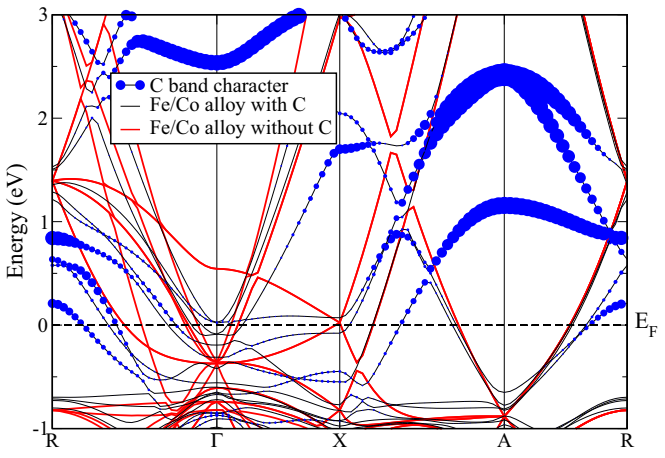

FIG. 4. (Color online) Comparison of the spin-up band structure of $(Fe_{0.4}Co_{0.6})_{16}C$ with undistorted $Fe_{0.4}Co_{0.6}$ with the same structural parameters a and c. C band character is highlighted.

IV. CONCLUSIONS

In conclusion, we have theoretically evaluated the structural and magnetic properties of Fe-Co alloys doped by carbon. A stable tetragonal distortion forms in a wide range of cobalt concentrations, which in turn gives rise to magnetocrystalline anisotropy energy well beyond the values of elemental iron, cubic cobalt, or their bulk alloys. The calculated values are instead close to that of hcp Co. For all considered alloys the saturation moment is larger than in hcp Co. Thus the material could display an increased energy product at reduced Co concentration.

Comparative study of MAE using various computational methods confirms that VCA leads to overestimated values. CPA gives more modest values, but relaxed supercells indicate that the species-dependent local disorder may enhance the MAE.

It is likely that the tetragonal distortion can be stabilized by other interstitial elements. In addition, a small amount of heavy elements might enhance the MAE via hybridization effects [45]. However, these directions are left for future studies.

ACKNOWLEDGMENTS

We acknowledge support from EU project REFREEPERMAG, the Swedish Research Council, the KAW foundation, ERC Grant No. 247062 (ASD), STANDUPP, and eSSENCE. Swedish National Infrastructure for Computing (SNIC), NSC Matter and Institute of Molecular Physics Polish Academy of Sciences, Poznan, Poland are acknowledged for computer resources.

[1] H. Fujii, T. Hokabe, T. Kamigaichi, and T. Okamoto, J. Phys. Soc. Jpn. **43**, 41 (1977).
[2] M. Costa, O. Grånäs, A. Bergman, P. Venezuela, P. Nordblad, M. Klintenberg, and O. Eriksson, Phys. Rev. B **86**, 085125 (2012).
[3] S. Bhandary, O. Grånäs, L. Szunyogh, B. Sanyal, L. Nordström, and O. Eriksson, Phys. Rev. B **84**, 092401 (2011).
[4] Y. Miura, S. Ozaki, Y. Kuwahara, M. Tsujikawa, K. Abe, and M. Shirai, J. Phys. Condens. Matter **25**, 106005 (2013).
[5] W. Coene, F. Hakkens, R. Coehoorn, D. B. de Mooij, and C. de Waard, J. Magn. Magn. Mater. **96**, 189 (1991).
[6] T. Burkert, L. Nordström, O. Eriksson, and O. Heinonen, Phys. Rev. Lett. **93**, 027203 (2004).
[7] G. Andersson, T. Burkert, P. Warnicke, M. Björck, B. Sanyal, C. Chacon, C. Zlotea, L. Nordström, P. Nordblad, and O. Eriksson, Phys. Rev. Lett. **96**, 037205 (2006).
[8] P. Warnicke, G. Andersson, M. Björck, J. Ferré, and P. Nordblad, J. Phys. Condens. Matter **19**, 226218 (2007).
[9] F. Yildiz, M. Przybylski, X.-D. Ma, and J. Kirschner, Phys. Rev. B **80**, 064415 (2009).
[10] I. Turek, J. Kudrnovský, and K. Carva, Phys. Rev. B **86**, 174430 (2012).
[11] C. Neise, S. Schönecker, M. Richter, K. Koepernik, and H. Eschrig, Phys. Status Solidi B **248**, 2398 (2011).
[12] N. Seljakow, G. Kurdjumow, and N. Goodtzow, Z. Phys. **45**, 384 (1927).
[13] G. Kurdumoff and E. Kaminsky, Nature (London) **122**, 475 (1928).
[14] G. Kurdjumov and E. Kaminsky, Z. Phys. **53**, 696 (1929).
[15] W. L. Fink and E. D. Campbell, Trans. Am. Soc. Steel Treat. **9**, 717 (1926).
[16] G. V. Kurdjumov and A. G. Khachaturyan, Acta Metall. **23**, 1077 (1975).
[17] G. V. Kurdjumov, Metall. Trans. Acta **7**, 999 (1976).
[18] P. Gustafson, Scand. J. Metall. **14**, 259 (1985).
[19] P. Trucano and R. Chen, Nature (London) **258**, 136 (1975).
[20] W. C. Ellis and E. S. Greiner, Trans. Am. Soc. Met. **29**, 415 (1941).
[21] S. Ohba, Y. Saito, and Y. Noda, Acta Crystallogr. A **38**, 725 (1982).
[22] P. E. Blöchl, Phys. Rev. B **50**, 17953 (1994).
[23] G. Kresse and D. Joubert, Phys. Rev. B **59**, 1758 (1999).
[24] G. Kresse and J. Furthmüller, Comput. Mater. Sci. **6**, 15 (1996).
[25] G. Kresse and J. Furthmüller, Phys. Rev. B **54**, 11169 (1996).
[26] J. P. Perdew, K. Burke, and M. Ernzerhof, Phys. Rev. Lett. **77**, 3865 (1996).
[27] H. J. Monkhorst and J. D. Pack, Phys. Rev. B **13**, 5188 (1976).
[28] O. K. Andersen, O. Jepsen, and G. Krier, in *Lectures on Methods of Electronic Structure Calculation* (World Scientific, Singapore, 1994), p. 63.
[29] O. K. Andersen, C. Arcangeli, R. W. Tank, T. Saha-Dasgupta, G. Krier, O. Jepsen, and I. Dasgupta, Mater. Res. Soc. Symp. Proc. **491**, 3 (1998).
[30] L. Vitos, H. L. Skriver, B. Johansson, and J. Kollár, Comput. Mater. Sci. **18**, 24 (2000).
[31] L. Vitos, Phys. Rev. B **64**, 014107 (2001).
[32] L. Vitos, I. A. Abrikosov, and B. Johansson, Phys. Rev. Lett. **87**, 156401 (2001).
[33] L. Vitos, J. Kollar, and H. L. Skriver, Phys. Rev. B **55**, 13521 (1997).
[34] J. Kollár, L. Vitos, and H. L. Skriver, in *Electronic Structure and Physical Properties of Solids: The Uses of the LMTO Method*, edited by H. Dreyssé, Lectures Notes in Physics Vol. 535 (Springer, Berlin, 2000), p. 85.
[35] P. Soven, Phys. Rev. **156**, 809 (1967).
[36] B. L. Györffy, Phys. Rev. B **5**, 2382 (1972).
[37] P. A. Korzhavyi, A. V. Ruban, I. A. Abrikosov, and H. L. Skriver, Phys. Rev. B **51**, 5773 (1995).
[38] P. Blaha, G. Madsen, K. Schwarz, D. Kvasnicka, and J. Luitz, *WIEN2k, An Augmented Plane Wave + Local Orbitals Program for Calculating Crystal Properties* (Karlheinz Schwarz, Techn. Universität Wien, Austria, 2001).
[39] H. J. F. Jansen, Phys. Rev. B **59**, 4699 (1999).
[40] H. Ebert, D. Ködderitzsch, and J. Minár, Rep. Prog. Phys. **74**, 096501 (2011).
[41] A. Zunger, S.-H. Wei, L. G. Ferreira, and J. E. Bernard, Phys. Rev. Lett. **65**, 353 (1990).
[42] A. van de Walle, P. Tiwary, M. de Jong, D. L. Olmsted, M. Asta, A. Dick, D. Shin, Y. Wang, L.-Q. Chen, and Z.-K. Liu, Calphad J. **42**, 13 (2013).
[43] E. K. Delczeg-Czirjak *et al*. (unpublished).
[44] N. Al-Zoubi, N. V. Skorodumova, A. Medvedeva, J. Andersson, G. Nilson, B. Johansson, and L. Vitos, Phys. Rev. B **85**, 014112 (2012).
[45] C. Andersson, B. Sanyal, O. Eriksson, L. Nordström, O. Karis, D. Arvanitis, T. Konishi, E. Holub-Krappe, and J. H. Dunn, Phys. Rev. Lett. **99**, 177207 (2007).